Journal of Quantitative Spectroscopy & Radiative Transfer 170 (2016) 90–105

Contents lists available at ScienceDirect

Journal of Quantitative Spectroscopy & Radiative Transfer

journal homepage: www.elsevier.com/locate/jqsrt

Observations of downwelling far-infrared emission at Table Mountain California made by the FIRST instrument

Martin G. Mlynczak [a,*], Richard P. Cageao [b], Jeffrey C. Mast [d], David P. Kratz [a], Harri Latvakoski [c], David G. Johnson [b]

[a] Climate Science Branch, Mail Stop 420, NASA Langley Research Center, Hampton, VA 23681-2199, United States
[b] Remote Sensing Flight Systems Branch, Mail Stop 468, NASA Langley Research Center, Hampton, VA 23681-2199, United States
[c] Space Dynamics Laboratory, 1695 Research Park Way, Logan, UT 84341, United States
[d] Science Systems and Applications Incorporated, 1 Enterprise Parkway, Hampton, VA 23666, United States

ARTICLE INFO

Article history:
Received 17 July 2015
Received in revised form
20 October 2015
Accepted 20 October 2015
Available online 27 October 2015

Keywords:
Far-Infrared
Spectral radiance
Water vapor
Greenhouse effect
Radiative closure

ABSTRACT

The Far-Infrared Spectroscopy of the Troposphere (FIRST) instrument measured downwelling far-infrared (far-IR) and mid-infrared (mid-IR) atmospheric spectra from 200 to 800 cm^{-1} at Table Mountain, California (elevation 2285 m). Spectra were recorded during a field campaign conducted in early autumn 2012, subsequent to a detailed laboratory calibration of the instrument. Radiosondes launched coincident with the FIRST observations provide temperature and water vapor profiles for model simulation of the measured spectra. Results from the driest day of the campaign (October 19, with less than 3 mm precipitable water) are presented here. Considerable spectral development is observed between 400 and 600 cm^{-1}. Over 90% of the measured radiance in this interval originates within 2.8 km of the surface. The existence of temperature inversions close to the surface necessitates atmospheric layer thicknesses as fine as 10 m in the radiative transfer model calculations. A detailed assessment of the uncertainties in the FIRST measurements and in the model calculations shows that the measured radiances agree with the model radiance calculations to within their combined uncertainties. The uncertainties in modeled radiance are shown to be larger than the measurement uncertainties. Overall, the largest source of uncertainty is in the water vapor concentration used in the radiative transfer calculations. Proposed new instruments with markedly higher measurement accuracy than FIRST will be able to measure the far-IR spectrum to much greater accuracy than it can be computed. As such, accurate direct measurements of the far-IR, and not solely calculations, are essential to the assessment of climate change.

1. Introduction

The climate of the Earth is maintained by incoming shortwave radiation from the Sun at wavelengths less than 4 μm and outgoing longwave radiation emitted by the Earth and its atmosphere between 4 and 100 μm. Presently all orbiting spectral resolving sensors that measure the top-of-atmosphere infrared Earth radiance do so between approximately 4 and 15.5 μm (2500–650 cm^{-1}), largely for the purposes of atmospheric temperature and moisture profiling for weather forecasting. Examples of these are the Atmospheric Infrared Sounder (AIRS) [1], the Infrared Atmospheric Sounding Interferometer (IASI) [2], and the Cross-Track Infrared Sounder (CrIS) [3] instruments.

* Corresponding author. Tel.: +1 757 864 5695.
E-mail addresses: m.g.mlynczak@nasa.gov (M.G. Mlynczak), richard.p.cageao@nasa.gov (R.P. Cageao), jeffrey.c.mast@nasa.gov (J.C. Mast), david.p.kratz@nasa.gov (D.P. Kratz), harri.latvakoski@sdl.usu.edu (H. Latvakoski), david.g.johnson@nasa.gov (D.G. Johnson).

http://dx.doi.org/10.1016/j.jqsrt.2015.10.017

Over the past 20 years several instruments [4–7] have been developed with the ultimate goal of measuring the Earth's far-infrared (far-IR, 15–100 μm) spectrum that is not presently observed directly from space. These instruments have observed the far-IR spectrum from the ground, from aircraft, and from high altitude balloons in the lower stratosphere. Concurrently, the importance of direct measurements of Earth's far-IR spectrum has become widely recognized [8]. The far-IR contains approximately one-half of the Earth's outgoing infrared radiation and greenhouse effect [9,10]. Earth's troposphere cools to space almost exclusively in this spectral region [11]. Cirrus clouds also have a strong radiative effect [12]. Numerous spectral fingerprints of climate change are found in the far-IR [13]. Consequently, measurements of the top-of-atmosphere far-IR spectrum are a critical component of the proposed NASA Climate Absolute Radiance and Refractivity Observatory (CLARREO) mission [14].

In this paper we present measurements of the downwelling far-IR and mid-IR emission spectrum of Earth's atmosphere recorded by the Far-Infrared Spectroscopy of the Troposphere (FIRST) instrument during a field campaign at Table Mountain, California, in late summer and early autumn 2012. FIRST was deployed to the Table Mountain Facility (TMF) after completing a re-calibration of the instrument earlier that year [15,16]. During the field campaign radiosondes were periodically launched from TMF to provide temperature and moisture profiles needed for radiative transfer model computations of the downwelling spectral radiance to compare with FIRST measurements.

The purpose of this paper is to present a comprehensive uncertainty analysis of the difference between the modeled radiance and the measured radiance (i.e., the measurement residual). Known uncertainties from the recent absolute calibration of the FIRST instrument are combined with the computed uncertainties in the modeled radiances to provide the uncertainty in the measurement residual. This "combined uncertainty" allows quantitative assessment of the degree to which radiative closure is attained. The approach defined here will also serve as the basis for analysis of other far-IR radiative closure experiments such as the RHUBC-II campaign [17]. We have found that the FIRST measurements and the radiative transfer model calculations agree to within their combined uncertainties and that the uncertainty in the modeled radiance is larger than the measurement uncertainty.

In the next section we describe the FIRST instrument and its recent calibration for ground-based observations. Atmospheric conditions during the observation period reported here are described, including their impact on radiative transfer calculations. Comparisons between measured and modeled radiances are given, along with the detailed analysis of uncertainties. A discussion and summary concludes the paper.

2. FIRST instrument description

The Far-Infrared Spectroscopy of the Troposphere (FIRST) instrument is a Fourier transform spectrometer (FTS) developed under the NASA Instrument Incubator Program for the purpose of demonstrating technology needed to measure the far-IR spectrum from a space-based instrument. FIRST was built in a partnership between the NASA Langley Research Center, the Space Dynamics Laboratory (SDL) of the Utah State University, and the Smithsonian Astrophysical Observatory. The instrument was initially designed to operate on a high altitude (~30 km) stratospheric balloon platform to simulate the measurement of top-of-atmosphere Earth radiance. The instrument successfully conducted an engineering demonstration flight in 2005 from the NASA balloon flight facility in Fort Sumner, New Mexico [6]. Measured radiance calibration was accomplished on-board during the flight by alternate views of an ambient temperature blackbody and a sky (or space) view through an open port. Subsequently, the instrument scene select assembly was modified to accommodate two calibration blackbodies (one heated above ambient temperature and one at ambient temperature) so as to enable FIRST to operate as a ground-based instrument and observe downwelling atmospheric radiance at Earth's surface. In 2009 FIRST participated in an atmospheric field campaign in the Atacama Desert in Chile [17]. Subsequent to this campaign FIRST was returned to SDL in late 2011 for absolute radiance recalibration in anticipation of future ground-based atmospheric observation campaigns. The instrument was calibrated in both the ground-based mode, with two calibration blackbodies [16], and in its stratospheric balloon operation mode, with an ambient blackbody and a liquid nitrogen cooled blackbody to simulate the space view from 30 km [15].

The FIRST instrument is described in the paper detailing the recalibration in ground-based configuration [16]. The interferometer is a porch swing design, recording double sided interferograms with a mirror travel of 0.5 cm either side of center (i.e., zero optical path difference). A helium-neon metrology laser is used to determine sampling location. FIRST samples every laser fringe and collects 24576 points for each interferogram. This results in 1.55 cm of total optical path difference change and 0.78 cm in total physical travel. After centering the interferogram and trimming the ends the realized spectral resolution is 0.643 cm^{-1}, corresponding to the distance from line center to the first zero of the sinc function instrument line shape. Data collection time for one scan is 11.5 s including turnaround time. The designed spectral coverage was 10–100 μm (1000–100 cm^{-1}) although the realized coverage spans 2200–50 cm^{-1}. The FIRST focal plane is comprised of 10 silicon bolometers cooled with liquid helium.

3. FIRST operations at Table Mountain, California

FIRST was deployed to the Table Mountain Facility (TMF, 34.4 °N, 117.7 °W, 2285 m) for eight weeks spanning August 2012 to October 2012. The TMF site is maintained by the NASA Jet Propulsion Laboratory. FIRST was operated at TMF inside a trailer that is used to transport it to and from field campaign sites. During measurements the trailer doors and windows were left open to keep the air inside the trailer at the same temperature as the outside

atmosphere, especially at night. The instrument views the atmosphere through an open port in the top of the trailer. The trailer was also unoccupied during atmospheric observations to further minimize temperature differences with the outside environment.

For routine observations FIRST was operated with a pre-programmed scan mode lasting approximately one hour. In this mode the instrument views both calibration blackbodies in turn, for approximately 5 min each, then views the atmosphere for approximately 30 min, then views the calibration blackbodies again for approximately 5 min each. This process was run several times each day or night of operation.

Vaisala RS92-SGPD radiosondes were launched to provide atmospheric temperature and moisture profiles from which atmospheric radiance spectra are computed for comparison with FIRST measurements. Typically the first radiosonde of the day was launched at the beginning of the first instrument sky-oriented view scan of the day. However, it takes approximately 90 min for the sonde to complete its ascent before the next sonde can be launched. Therefore, typically two sets of FIRST atmospheric observations and calibration blackbody views completed for each radiosonde flight. FIRST observations were made day and night during the TMF deployment period. Measurements were made during clear sky conditions and partially cloudy sky conditions. The results reported here for October 19 are entirely at night with an exceptionally clear sky and low integrated precipitable column water vapor.

The TMF is equipped with a ground-based GPS receiver that provides estimates of integrated precipitable water (IPW) above the site. Fig. 1 shows the time series of IPW from the GPS receiver at TMF from September 13 to October 24 2012 during the FIRST TMF campaign. The available values reported are the median IPW for a 30-min interval. The lowest observed IPW of ~0.20 cm was in the period around October 19–21 2012. The greatest spectral development in the far-IR occurs with the lowest IPW amounts. For this reason we chose the set of clear-sky spectra from October 19 2012 to analyze and present here.

4. FIRST data preparation and instrument calibration

4.1. Detector selection

The FIRST instrument focal plane consists of a sparsely populated square array of 10 silicon bolometer detectors behind Winston cone compound parabolic concentrators. The size of the focal plane is 3.8 cm by 3.8 cm. Two detectors are located at the center of the focal plane and two are located at each corner. The detectors were arranged this way to demonstrate far-IR imaging with a Fourier transform spectrometer instrument, without having to provide the full 100 detectors for which the focal plane was sized. In the ground-based instrument configuration, looking upward at the zenith, radiance measurements calibrated with the two temperature point instrument reference blackbodies should produce equivalent results for all 10 detectors. As this was not entirely the case, six detectors were chosen from the 10-element ensemble, based on observed zenith sky spectral analysis (in spectral windows and fully absorbed radiance regions) and on instrument laboratory reference blackbody calibration [15,16]. Radiances measured with this subset of detectors were also corrected for bolometer response non-linearity [15]. For each detector a mean spectrum is obtained by averaging the approximately 150 individual spectral taken during a 30-min atmospheric observation interval. These 30-min averages are reported here and compared with radiative transfer model calculations.

The detectors selected from FIRST's 10-detector array are detector numbers 2, 3, 4, 5, 6, and 8, all of which are all located at the corners of the focal plane. These selected detectors tracked one another, measuring radiances that agreed to better than 1%, particularly outside the narrow spectral far-IR windows where atmospheric brightness temperatures dropped below 180 K. The central two detectors, 1 and 10, were unusually noisy, with high background signal in laboratory calibrations both in 2011 and 2013 [15,16]. The noise resulted in spectra that were difficult to phase correct and match to calibration blackbody spectra and therefore questionable calibrated radiances are

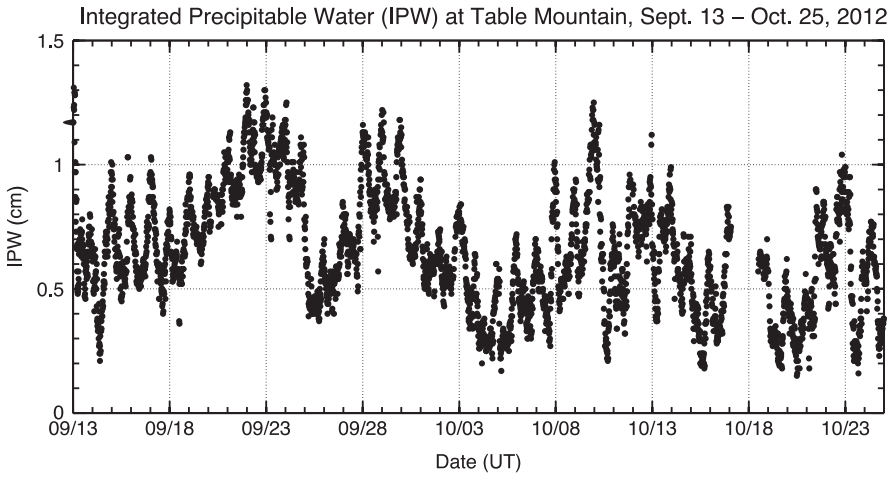

Fig. 1. Total integrated precipitable water (IPW) measured by the ground-based GPS receiver at TMF from September 13–October 25, 2012.

produced for these two detectors. Thus detectors 1 and 10 were therefore rejected from the ensemble average. Detector 9 tended to track these rejected detectors, particularly in the low radiance windows of the TMF data sets, as did detector 7, which lay outside the radiances of detectors 2, 3, 4, 5, 6, and 8. These six detectors tended to create a tight cluster of calibrated spectral radiances even in the low radiance window regions. A space view source scene calibration from the 2005 balloon flight also showed detector 7 with a significant out-of-family background signal, perhaps indicating high levels of observed stray light at this detector. For these reasons, detectors 7 and 9 were also rejected from the ensemble average.

4.2. FIRST laboratory calibration summary

FIRST was calibrated for absolute radiance measurement by attaching the Long Wave InfraRed Calibration Source (LWIRCS) [http://www.sdl.usu.edu/downloads/lwircs.pdf], a specular trap blackbody (painted with LORD Corporation Aeroglaze® Z302 paint) to the third port of its evacuated scene select assembly. The other two ports were occupied by radiometric calibration sources used during FIRST atmospheric measurements, either a warm (45 °C above ambient) and an ambient temperature source for ground-based calibration, or a warm and a liquid nitrogen cooled (space view simulator) source for balloon-borne deployment calibration. LWIRCS performance is calculated from a cavity model, Z302 paint measurements, and three NIST-calibrated temperature sensors. The emissivity is calculated to be greater than 0.9998 from 1–35 μm and greater than 0.9980 from 35 to 100 μm. The temperature uncertainty is 160 mK at 180 K, falling to 50 mK for 273 K and warmer. Output of the LWIRCS has been measured with the National Institute of Standard and Technology (NIST) transfer radiometer (TXR) at 5 and 10 μm. When observed with the TXR, the LWIRCS brightness temperature agrees with the LWIRCS temperature to within 95 mK (maximum deviation) at 5 μm from 210 to 350 K, and to within 186 mK at 10 μm from 180 to 350 K [18]. This level of agreement is within the TXR measurement uncertainty.

FIRST was calibrated over a range of geophysically relevant scene temperatures from 169 K to 310 K (in steps of approximately 20 K) and the systematic and random uncertainties were determined at each step. The 1-sigma results of this calibration [15,16] over the 200 to 800 cm^{-1} spectral range are shown here in Table 1, for ground-based operations.

The systematic uncertainty is better than 1 K for scene temperatures greater than 247 K, and it is between 1.0 and 2.6 K for scene temperatures between 209 and 247 K. The calibration uncertainty increases as scene temperature decreases in part due to calibration error propagation as the scene temperature gets further away from the warm (324 K) and ambient (293 K) calibration blackbody temperatures. The FIRST absolute accuracy in the balloon-borne observing configuration was higher at the low temperatures due to the lower temperature liquid nitrogen cooled calibration source. In the balloon configuration, accuracies of 0.5 K were recorded for 180–205 K scene temperatures, and 0.5–0.35 K from 200 to 325 K [15].

Table 1
FIRST absolute radiometric calibration and noise performance from 200 to 800 cm^{-1}.

Scene temp.	Systematic error (K)	Random error (K)
310.3	0.2	0.10
292.7	0.2	0.10
270.5	0.3	0.34
247.4	1.0	1.0
228.2	1.2	0.70
225.2	1.5	1.3
209.4	2.6	2.2
189.3	3.5	1.5
169.1	4.5	4.1

A small bolometer response non-linearity was discovered serendipitously in a different far-IR interferometer at NASA Langley in early 2013. This non-linearity is caused by heating of the bolometer, attributable to changes in incident radiance across the wide 5–50 μm spectral band incident on the bolometer, which causes a reduction in resistance and changes in the detector gain as the instrument switches from scene to calibration sources which are at different temperatures. A voltage change in the bolometer readout circuit is proportional to the detector resistance and the response non-linearity is corrected by scaling proportional to the bolometer DC voltage. This correction removes most of the prior [16] deviation between the FIRST observed and LWIRCS temperature. FIRST data from TMF are now corrected for this non-linearity and this is reflected in the values shown in Table 1 above.

4.3. Radiative transfer model calculations

To analyze the measured FIRST spectra, modeled spectra are calculated using the AER Line-by-Line Radiative Transfer Model (LBLRTM) [19], version 12.2, developed by AER Corporation. Spectral line parameters used in LBLRTM are Version 3.2 of the line parameter database provided by AER Corporation. The water vapor continuum is computed using the MT-CKD 2.5.2 continuum model. We also present some calculations performed with the Monochromatic Radiative Transfer Algorithm (MRTA) model [20,21].

Temperature and moisture profiles for input to the radiative transfer codes are measured by the radiosondes launched during FIRST observing periods. The radiosonde profiles contain pressure (hPa), temperature (K), and water vapor specific humidity (g/kg) as a function of altitude, sampled every two seconds through a roughly 90 minute flight. The radiosonde profiles are combined with profiles of CO_2 (391 ppm), O_3, N_2O, CO, CH_4, and O_2 obtained from a standard mid-latitude summer atmosphere to complete the input for LBLRTM (and MRTA).

The simulated spectra are calculated at much higher resolution (0.0014 cm^{-1}) than the FIRST spectral data (0.643 cm^{-1}). To enable comparison of the measured and modeled spectra, the LBLRTM spectra are convolved with the line shape of the FIRST instrument and output on the FIRST wavenumber grid. A simple 3-point Hamming apodization using a triangle window function is also applied to both FIRST and LBLRTM spectra to reduce the effects of ringing due to the instrument (sinc function) lineshape

and insure direct model/data comparisons. FIRST data at each spectral wavenumber are averaged for six detectors and then approximately 150 individual 11.5 s interferometer scans were averaged in produce the standard 30 min data product shown here. In the results shown below FIRST 30-min averages are compared with LBLRTM calculations based on the radiosonde profile coincident with the start of the 30 min FIRST observation period. We note that the radiosonde passes through more than 50%, 75%, and 95% of the integrated precipitable water vapor in 3 min, 9 min, and 25 min of ascent, respectively, recording temperature and water vapor every 2 s.

Table 2
Listing of date, sonde launch time, FIRST scan start time, and sonde IPW for FIRST observations on October 19, 2012.

Date	Sonde Launch (UT)	FIRST scan start (UT)	Sonde IPW (cm)
10/19/2012	7:15	07:05	0.300
10/19/2012	8:56	08:46	0.308
10/19/2012	10:36	10:27	0.311
10/19/2012	12:17	12:07	0.289

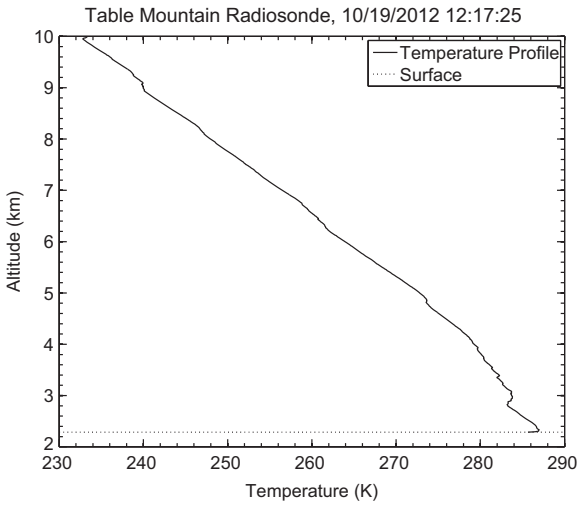

Fig. 2. Temperature profile below 10 km measured by the Vaisala RS92 radiosonde launched at 12:17 UT. The dotted horizontal line indicates the altitude of the surface above sea level.

5. Results

5.1. Atmospheric conditions

Results are presented here for October 19, 2012 at TMF. The first sonde was launched at 07:15 UT, which corresponds to 00:15 local time, i.e., just after midnight. Listed in Table 2 are the launch times of four sonde flights over a 5-h period and the corresponding time that the FIRST instrument started calibration, which is approximately 10 min before atmospheric observations started. Clear sky conditions were observed during the entire period reported here. The integrated precipitable water vapor derived from each sonde flight is listed. Over the six hours covered by the four sonde launches, the sonde-measured IPW varied by as much as 7.5%.

Shown in Fig. 2 is the temperature profile below 10 km measured by the radiosonde launched at 12:17 UT. Recall that the surface at Table Mountain Facility (TMF) is at 2285 m above sea level.

Shown in Fig. 3 is the temperature profile up to 1 km above the ground at TMF from the same sonde. Note the existence of two small but significant inversions just above ground. Modeling this inversion accurately in the radiative transfer calculations is essential to achieving agreement between the observed and computed radiances in the optically thick portion of the spectrum, particularly in the

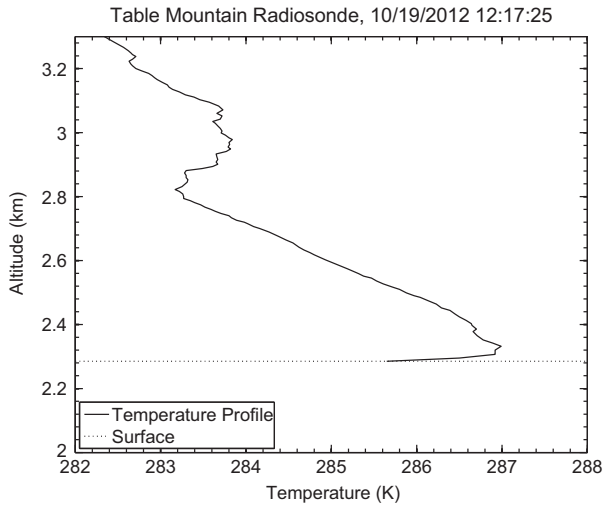

Fig. 3. Radiosonde measured temperature profile approximately up to 1 km above the surface at TMF at 12:17 UT. The existence of two inversion layers, one peaking at about 40 m above the surface, and the other near 3 km altitude (700 m above the surface), strongly influence the layering required in the radiative transfer calculations.

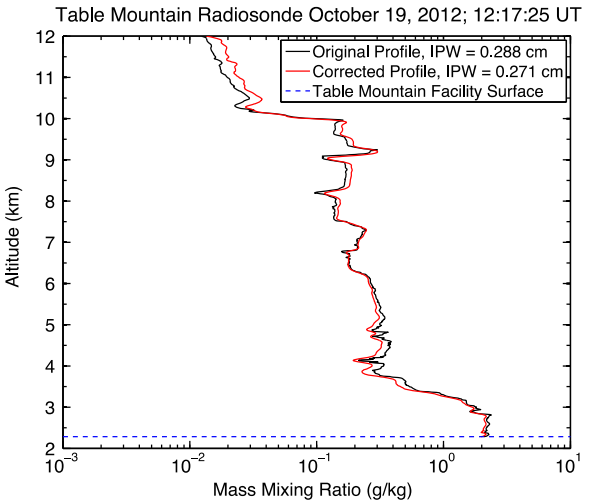

Fig. 4. Water vapor mass mixing ratio (g/kg) profile measured by the sonde launched at 12:17 UT. The black curve is the measured profile, the red curve is the mixing ratio profile after application of the Miloshevich correction. The horizontal dotted line represents the altitude of the TMF facility (2.285 km).

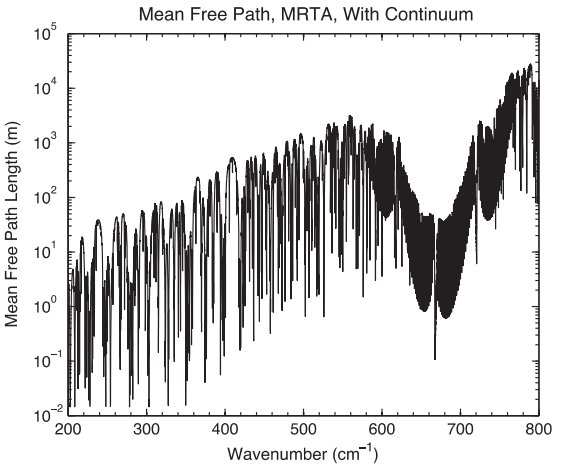

Fig. 5. Mean free path (m) as a function of wavenumber for a vertically traveling photon leaving the surface at Table Mountain, for surface conditions at 12:17 UT, computed with the MRTA code [20,21].

15 μm CO_2 bands that saturate just above the instrument, as discussed below.

Fig. 4 shows the water vapor mass mixing ratio profile measured by the 12:17 UT sonde (black curve) and the profile after application of a Miloshevich [22] Vaisala RS92 sonde water vapor bias correction (red curve). The correction accounts for known sonde biases, as determined by comparison with cryogenic frost point hygrometers, and for time lags of the sonde sensor. The effect of this Miloshevich correction for the conditions during our TMF campaign was to reduce the water vapor mass mixing ratio at low altitudes and increase it at higher altitudes. Overall the correction decreases the 12:17 UT sonde-measured IPW from 0.289 cm to 0.271 cm, a 6.5% reduction. This is an especially important consideration for the ground-based measurements made by FIRST. One half of the IPW is in the first 750 m above the instrument; 75% of the IPW is 2135 m above the instrument; and 90% of the IPW is 4450 m above the instrument (i.e., below an altitude of 6735 m). The Miloshevich correction reduces the water vapor amounts in the region of the atmosphere where the FIRST radiance originates. All comparisons between FIRST observations and LBLRTM simulated radiances use water vapor profiles with the Miloshevich correction applied. The corrected profile also has an established accuracy and uncertainty that will be used in assessing the agreement between FIRST measurements and modeled radiances.

5.2. Consequences of atmospheric structure for radiative transfer modeling

The unique nature of ground-based observations and the atmospheric structure on this day, particularly with the presence of an inversion layer tens of meters in depth, has a profound effect on the calculation of radiative transfer. To illustrate this fact, we begin by assessing the opacity of the atmosphere by computing the mean free path of photons leaving the surface and traveling in the zenith direction. The mean free path considered here is the distance required to achieve unit optical depth at the spectral frequency of the photon for conditions at the surface.

Fig. 5 shows the mean free path computed with the MRTA code at 0.005 cm^{-1} resolution. Between 500 and 600 cm^{-1} the mean free path can be as long as several km, indicating that the atmosphere should be quite transparent within this region. However, for much of the region between 200 and 800 cm^{-1} the mean free path is under 100 m. This means that the atmosphere in such regions is effectively opaque within 100 m or so above the FIRST trailer. The existence of short mean free paths through the inversion layer requires us to divide the atmosphere fine layers, as thin at 10 m, to accurately reproduce the thermal structure in the LBLRTM model simulation of the FIRST radiance. The lowest 115 m of the atmosphere required seven layers ranging in thickness from 10 to 23 m in order to capture the atmospheric structure and produce radiances that agree well (as shown below) with the FIRST measurements.

In addition there are multiple very strong absorption features in which the mean free path is less than 0.1 m (10 cm). For these features absorption occurs inside the FIRST instrument, since there is approximately 18 cm of path from the instrument scene select mirror to the entrance aperture of the instrument. Due to the warm blackbody, the path in the instrument can be 5–7 K hotter than the ambient air temperature, based on temperature sensor on the FIRST scene select mirror. For example, at 667 cm^{-1}, the CO_2 band center, the mean free path is 10 cm, and thus there is considerable absorption inside the FIRST instrument at this wavenumber. Radiance from inside the instrument at 667 cm^{-1} is evident in the FIRST measurements and a technique to account for this is described below.

Shown in Fig. 6a is the measured (30 min average) FIRST spectrum recorded from 12:18 to 12:47 UT on 19 October 2012. This spectrum is representative of all the spectra taken

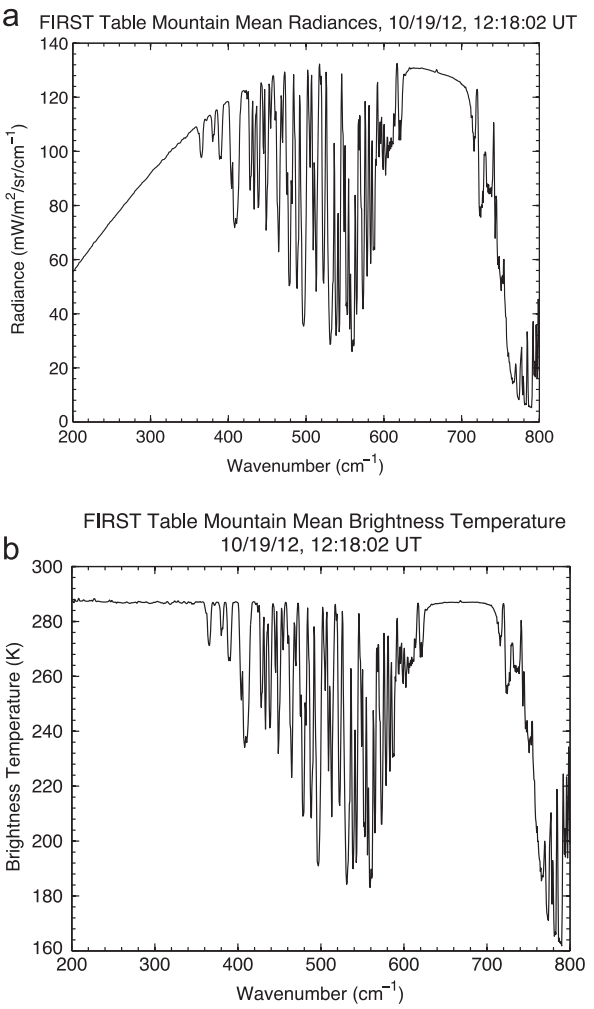

Fig. 6. (a) FIRST radiance spectrum measured at Table Mountain, CA, October 19, 2014. Thirty minute average spectrum of 150 individual spectra, beginning at 12:17 UT. (b) FIRST brightness temperature spectrum derived from Fig. 6a. The lowest brightness temperature in the far-IR is approximately 185 K near 560 cm^{-1}.

the rest of the evening due to the low variability of water vapor and temperature. Fig. 6b shows the same spectrum but in brightness temperatures. As expected from the mean free path figure and discussion, the radiance in the far-IR between 200 and 360 cm^{-1} and in the core of the 15-μm band is essentially that of a blackbody spectrum at the near-surface air temperature (285.65 K). Substantial spectral development is observed in the 400–600 cm^{-1} region, with brightness temperatures as low as 185 K observed.

To fully understand the origin of the radiation measured in the 400–600 cm^{-1} region we computed the cumulative contributions of radiance from each layer of atmosphere to the total radiance at four different wavenumbers (408.49, 465.06, 496.55, and 558.90 cm^{-1}) that span a range of brightness temperatures from 235 K to 190 K, based on the temperature and water vapor profiles observed with the 12:17 UT sonde. Ninety percent of the radiance at these four wavenumbers arises in the atmosphere at 1134 m, 1607 m, 1851 m, and 2833 m above the

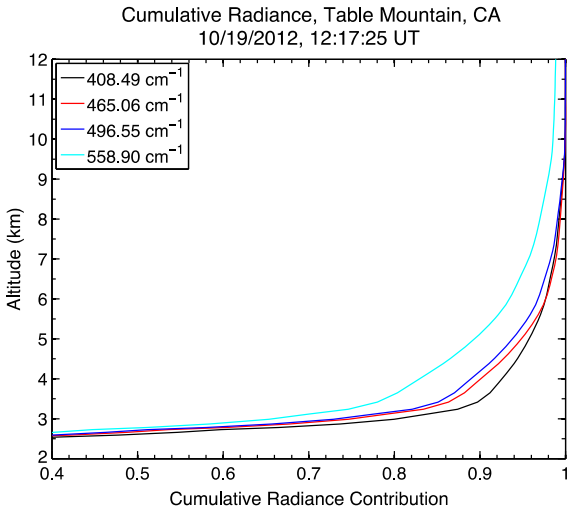

Fig. 7. Cumulative radiance contribution to the total surface radiance at four different wavenumbers spanning a wide range of atmospheric opacity. Ninety percent of the measured radiance originates between 1.1 km and 2.8 km above the instrument.

surface, respectively. This can be seen in Fig. 7 below. The sonde traverses these distances in 280 s, 408 s, 471 s, and 727 s, respectively. The 558.9 cm^{-1} interval still has fractional contributions to the total radiance above 10 km. From this figure we conclude that 90% of the radiance measured by FIRST between 200 and 800 cm^{-1} arises within 2833 m above the instrument.

6. Comparison of FIRST and calculated radiances

The goal of the deployment to TMF was to record radiances with the FIRST instrument and compare them with line-by-line radiative transfer models in order to assess the understanding of water vapor spectroscopy in the far-IR. The key element of this comparison is an assessment of the uncertainty in the measurements and in the model calculations. The degree of agreement or disagreement between measured and modeled radiances, and hence achievement of radiative closure, can only be diagnosed through a consideration of the respective uncertainties of the instrument and the model.

As mentioned previously, some very strong lines of CO_2 and H_2O have large absorption within the FIRST foreoptics, as there are 18 cm between the entrance aperture and the scene select mirror. The hot blackbody used for calibration effectively produces warm air over this 18 cm and just above the entrance aperture to the instrument. Temperature sensors on the scene select mechanism indicated this air is approximately 5–7 K warmer than the ambient air temperature. To simulate the radiance on the FIRST scene select mirror, we add an 18 cm “hot path” layer to the line-by-line radiance calculation for comparison with the measured FIRST radiance. This approach, given in Eq. (1) for monochromatic radiation, accounts for the transmission of atmospheric radiance through the layer and for emission within the layer. R_{in} is the radiance on the FIRST scene select mirror, R_{LBL} is the line-by-line radiance

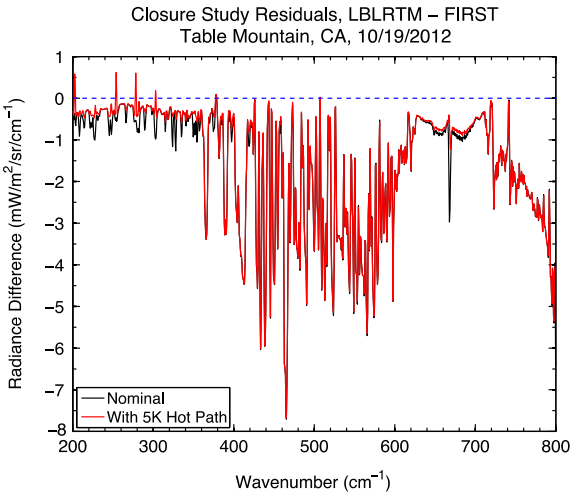

Fig. 8. Radiance difference, LBLRTM minus FIRST, with and without correction for the 18 cm hot path 5 K above ambient temperature within the instrument. The effects are largest in the far-IR (200–360 cm^{-1}) and in the core of the 15-μm CO_2 band where opacities are greatest.

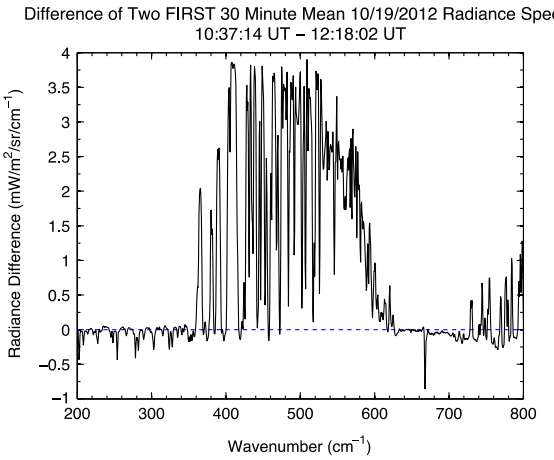

Fig. 9. Maximum radiance difference measured by FIRST on 10/19/2012.

calculated based on measured atmospheric temperature and moisture profiles from the radiosonde, T_p is the temperature of the 18 cm hot path, and τ and ε are the transmissivity and emissivity of the hot path. The emissivity is evaluated based on ambient relative humidity and CO_2 abundance (391 ppm).

$$R_{in} = R_{LBL} * (\tau) + \epsilon * B(T_p) \quad (1)$$

Shown in Fig. 8 (for the FIRST data collection sequence beginning at 12:07 UT) are the differences between FIRST and line-by-line calculated radiances only (black curve) and FIRST and hot-path corrected line-by-line radiances (red curve), for a hot path at 5 K above ambient. The hot path layer correction gives much better agreement in the optically thick regions, particularly in the core of the 15 μm CO_2 band.

6.1. Comparison of measured and modeled radiances

On October 19 2012 four sondes were launched as indicated in Table 2. During each sonde flight two FIRST measurement sequences (calibration and atmospheric observations) are completed, providing 8 sets of calibrated, 30-min, six detector averaged sky spectra for comparison with line-by-line radiance calculations from the 4 sonde flights. The radiances did not change substantially over the course of the evening as the precipitable water vapor was stable, changing by 7.5% at most, between the third and fourth sondes. Shown in Fig. 9 is the difference between the FIRST measured radiance for scans beginning at 10:37 UT and 12:18 UT, corresponding to the time period when the water vapor IPW decreased by 7.5% as measured by the radiosondes.

For each of the four sonde flights, we show comparisons with the first scan made by FIRST during each of the 4 sonde flights. This will give the closest correspondence in time between the observed water vapor and temperature and the observed spectra. Shown in Fig. 10 are the differences (line-by-line calculations using LBLRTM) and FIRST measured radiances for these four cases, spanning over five hours in time. The calculated and measured radiances agree most closely in the previously-discussed optically thick regions, from 200 to 360 cm^{-1} and between 620 and 700 cm^{-1}. In these regions the radiance differences range from 0.25 to 0.5 $mW/m^2/sr/cm^{-1}$, which correspond to brightness temperature differences of 0.16–0.4 K, which will be shown to be within the combined measured and modeled radiance uncertainty.

The largest observed differences in the calculated and measured radiances occur between 360 and 620 cm^{-1} where water vapor is the dominant absorbing species. As indicated in the mean free path discussion and Fig. 5, the water vapor absorption is relatively weak in this region. The transitions in this spectral interval are generally highly forbidden [23] and the spectral line parameters have changed substantially in the last 4 editions of the HITRAN database [24]. The observed differences are generally between 2 and 5 $mW/m^2/sr/cm^{-1}$, depending on wavenumber. There is one feature near 462 cm^{-1} that consistently exhibits the largest disagreement with FIRST radiances, approaching 7 $mW/m^2/sr/cm^{-1}$. We also note that the differences between 400 and 600 cm^{-1} are negative, meaning that the FIRST measured radiance is always larger than the modeled radiance. Although not shown, comparisons that used sonde water vapor profiles without the nighttime RS92 sonde Miloshevich correction were generally of the same magnitude but there was no definite offset around the zero difference line. As noted previously, the Miloshevich correction reduces the integrated precipitable water by 6.5%, thus reducing the calculated radiance in the far-IR.

To assess the level of agreement between model and data, the differences between them must be judged in light of the uncertainties in the FIRST measurements and in the modeled radiances. The data set can then assessed to determine whether it is sufficient to judge whether radiative closure has been achieved. There are many sources of

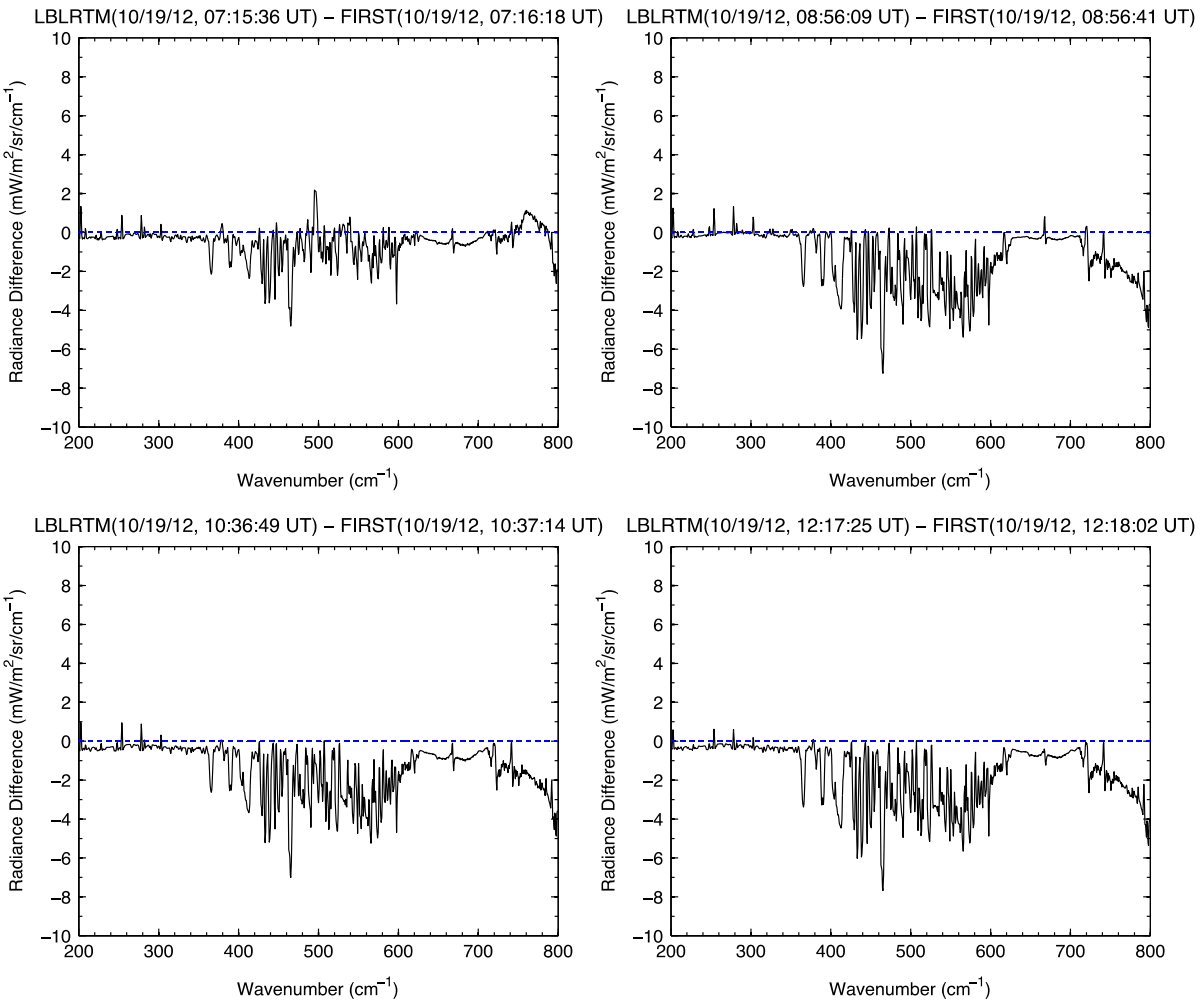

Fig. 10. Difference between FIRST measured radiances and radiances modeled based on observed temperature and water vapor concentrations from radiosondes.

measurement and modeling uncertainty and investigation of these will be the topic of the next section.

6.2. Uncertainty in measured and modeled radiance, and in their difference

To assess the level of agreement between FIRST and model radiance calculations, we evaluate the uncertainty in both the measured and modeled radiances. The individual sources of uncertainty considered here are assumed to be uncorrelated. Individual uncertainty terms are assessed separately for the measured and modeled radiances and are shown below. The total measurement uncertainty is computed as the root-sum-square (RSS) of the individual measurement uncertainties. Similarly, the total model uncertainty is computed as the RSS of the individual model uncertainties. We define the "combined" uncertainty as the RSS of the total model uncertainty and the total measurement uncertainty. The combined uncertainty is representative of the uncertainty in the difference of the measured and modeled radiances. We will now examine the uncertainty of the measured and modeled radiances in turn.

6.2.1. Uncertainty in FIRST measured radiances

There are three terms that comprise the individual uncertainty components of the FIRST measured radiance. They are: absolute radiometric calibration, detector-to-detector variations, and scene variability over a 30-min observing period. Absolute radiometric calibration, which represents the one standard deviation difference between FIRST and known radiance sources, is given in Table 1. These represent the average of the values for the FIRST detectors used in the comparison. However, there are minor differences in the radiances measured by each of the six detectors used to generate the FIRST radiances for comparison with the model calculations. The detector uncertainty is defined as the standard deviation of the detector radiances over 30 min. Prior to calculating the standard deviation, the mean radiance of each detector in the 30-min scan window is calculated. The detector uncertainty is then the standard deviation of these six mean radiance spectra. The sky uncertainty is defined as

the variability of the measured scene radiance in each 30-min period of atmospheric observations. During this time there are approximately 150 scans of 11.5-s duration, for which each of the six detectors considered records a spectrum. An average spectrum using the six detectors is computed for each 11.5 s scan, and the standard deviation of these spectra is computed using all 150 scans. This standard deviation is defined as the sky variability.

Lastly, random measurement noise is in principle another source of measurement uncertainty, and instantaneous values are given in Table 1. However, as the FIRST spectra reported here are averages in each spectral bin of 150 spectra taken over 30 min, the random noise is reduced substantially (by square root of 150) for the range of brightness temperatures observed. Consequently, random noise is not a significant component of overall measurement uncertainty.

Shown in Fig. 11 are the uncertainties for calibration, detector uncertainty, and sky uncertainty, in radiance units. Laboratory calibration (Table 1) is the largest source of uncertainty while sky variability over 30 min is quite small. The calibration uncertainty is largest in the optically thinner regions between 360 and 620 cm^{-1} and 720–800 cm^{-1} where the measured radiances are smaller, and thus have lower associated brightness temperatures, and hence larger calibration uncertainties, as shown in Table 1.

6.2.2. *Uncertainty in modeled radiances and combined measurement and model uncertainty*

The FIRST measurements are compared with radiances computed with the LBLRTM radiative transfer model. There are seven sources of uncertainty in the modeled radiance that are considered: Line strength and halfwidth uncertainties for water vapor; line strength and halfwidth uncertainties for carbon dioxide; uncertainty in the water vapor continuum; and uncertainties in the measured water vapor and temperature profiles. The uncertainties in the line strengths and line halfwidths are specified on the AER spectral line database. For example, for water vapor, between 200 and 800 cm^{-1}, there are 3638 lines on the AER v3.2 spectral line database. A total of 2205 of these lines comprise 99.7% of the total band strength in this

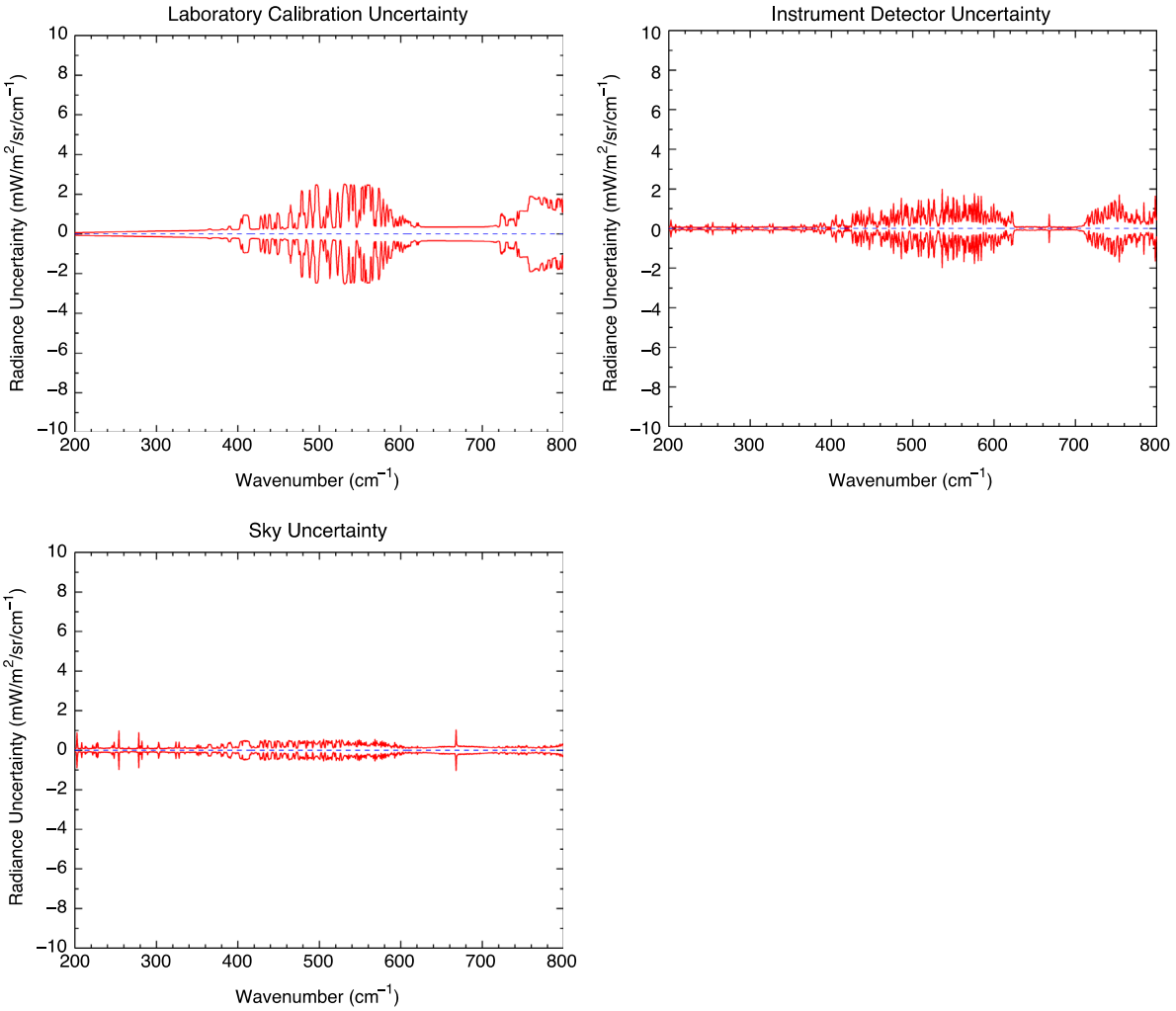

Fig. 11. Uncertainty in the FIRST measured radiances including calibration uncertainty (as per Table 1), detector-to-detector uncertainty, and variability of the sky/scene during the 30 min observation period.

Table 3
Uncertainties in the self and foreign broadened continua for water vapor.

Self continuum uncertainties		Foreign continuum uncertainties	
Range (cm^{-1})	Uncertainty	Range (cm^{-1})	Uncertainty
80–350	(+/−25%)	80–300	(+/−25%)
350–600	(+/−20%)	300– 400	(+/−20%)
600–800	(+/−10%)	400–600	(+/−15%)
		600–800	(+/−10%)

interval. These 2205 lines are listed as having uncertainties between 5% and 10%, for which we take an average of 7.5% in the uncertainty assessment here.

We use these uncertainties to estimate the uncertainty in the modeled radiance as follows. For example, for water vapor line strengths, we increase all of the line strengths on the line list by their specified uncertainty, and compute the radiance. We then take the difference between this "perturbed" radiance and the original modeled radiance, to obtain a spectrum of radiance uncertainty associated with the uncertainty in the line strengths. We then decrease all water vapor line strengths by the stated uncertainty, and compute the difference with the original modeled radiance. This provides an envelope of spectral radiance uncertainty based on the specified uncertainties in the water vapor line strengths. This approach is then followed for the water vapor halfwidths, the carbon dioxide line strengths, and the carbon dioxide half widths.

In addition to the uncertainties associated with the water vapor line parameters, there are uncertainties associated with the water vapor continuum formulation. To account for the uncertainties in the continuum, which are present in both the self and foreign water vapor coefficients, we used estimates of the uncertainties in the derived water vapor continuum coefficients provided by E. Mlawer (AER Corp., private communication), see Table 3. This allowed for calculations of the radiative impact of the uncertainties in the water vapor continua, which could then be combined with the other uncertainties.

Shown in Fig. 12 are the radiance uncertainties associated with the spectral line parameters for water vapor and carbon dioxide, and due to the water vapor continuum in the far-IR. The uncertainty in all cases exists only where there is spectral development in the observed spectrum. Those regions that are optically thick (200–360 cm^{-1} and 620–720 cm^{-1}) have no sensitivity to the line parameters at the specified uncertainties. Of these sources, the uncertainty in the water vapor line strengths is the largest individual uncertainty associated with spectral line parameters.

The model uncertainties associated with the water vapor and temperatures measured by the radiosondes are shown in Fig. 13. The water vapor uncertainty (left plot in Fig. 13) is derived from the sonde water vapor profile uncertainty after applying the Miloshevich [22] correction. Specifically, as given in [22], the uncertainty in the corrected water vapor relative humidity profile is +/−4% of the relative humidity value plus an additional 0.5% in relative humidity. For example, if the corrected relative humidity is 20%, the uncertainty is 4% of 20% (thus 0.8%) plus an additional 0.5% in relative humidity, for a total uncertainty of 1.3% in relative humidity (i.e., 20% +/−1.3%). This uncertainty, when integrated over the entire profile, results in a 10% uncertainty in the integrated precipitable water. In contrast, dedicated field experiments [25,26] have had ground-based microwave radiometers to observe the integrated precipitable water to an accuracy of 2% to compensate for the relatively large uncertainty in radiosonde data. The temperature profile uncertainty is 0.25 K from the data provided by the sonde manufacturer. The uncertainty envelopes in Fig. 13 are obtained by computing modeled radiances with and without the uncertainties, and taking their difference. Comparison of Figs. 11–13 shows that the water vapor is the largest individual source of uncertainty.

The next step is to compute the total uncertainty of the FIRST measurement and the total uncertainty of the modeled radiances. This is accomplished by computing the RSS of the measurement uncertainties in Fig. 11 and the RSS of the model uncertainties in Figs. 12 and 13. Shown in Fig. 14 are the total measurement uncertainties and the total model uncertainties. It is immediately evident that the uncertainty in the modeled radiance is the dominant source of uncertainty in this comparison, substantially exceeding the measurement uncertainty, particularly in the far-IR region between 360 and 620 cm^{-1}. An immediate conclusion is that the far-IR spectrum can be measured more accurately than it can be modeled, even with the relatively large calibration uncertainty of the FIRST instrument. Fig. 12 shows that the uncertainties due to spectroscopy (line strength, halfwidth, and continuum) rival and exceed that of the FIRST instrument calibration.

The final step prior to assessing the agreement between the measured FIRST spectra and the modeled radiances is to compute the combined uncertainty, which represents the combined effects of measurement and model uncertainties. As we assume that the measurement and model uncertainties are uncorrelated, the total combined uncertainty is taken to be the RSS of the total measurement uncertainty and the total model uncertainty shown in Fig. 14. The combined uncertainty is shown in Fig. 15, and is representative of the uncertainty in the difference between the FIRST measurements and LBLRTM computed radiances. This is the uncertainty envelope for comparing the model-measurement residuals, i.e., the difference between the LBLRTM radiative transfer calculations and the FIRST measurements.

7. Comparison of measurement and model residuals and combined uncertainties

Shown below in Fig. 16 are the residual radiances, that is, the LBLRTM model radiances minus the observed FIRST radiances (black curves), along with the combined measurement and model uncertainty shown in Fig. 15. The residual radiances are those shown in Fig. 10. Over the entire 200–800 cm^{-1} region, the model-measurement residual falls within the combined uncertainty envelope at all but a few spectral points. The most conspicuous is a feature near 465 cm^{-1}, in which the FIRST radiance is as much as 7 mW/m^2/sr/cm^{-1} larger than the model calculations. There is also

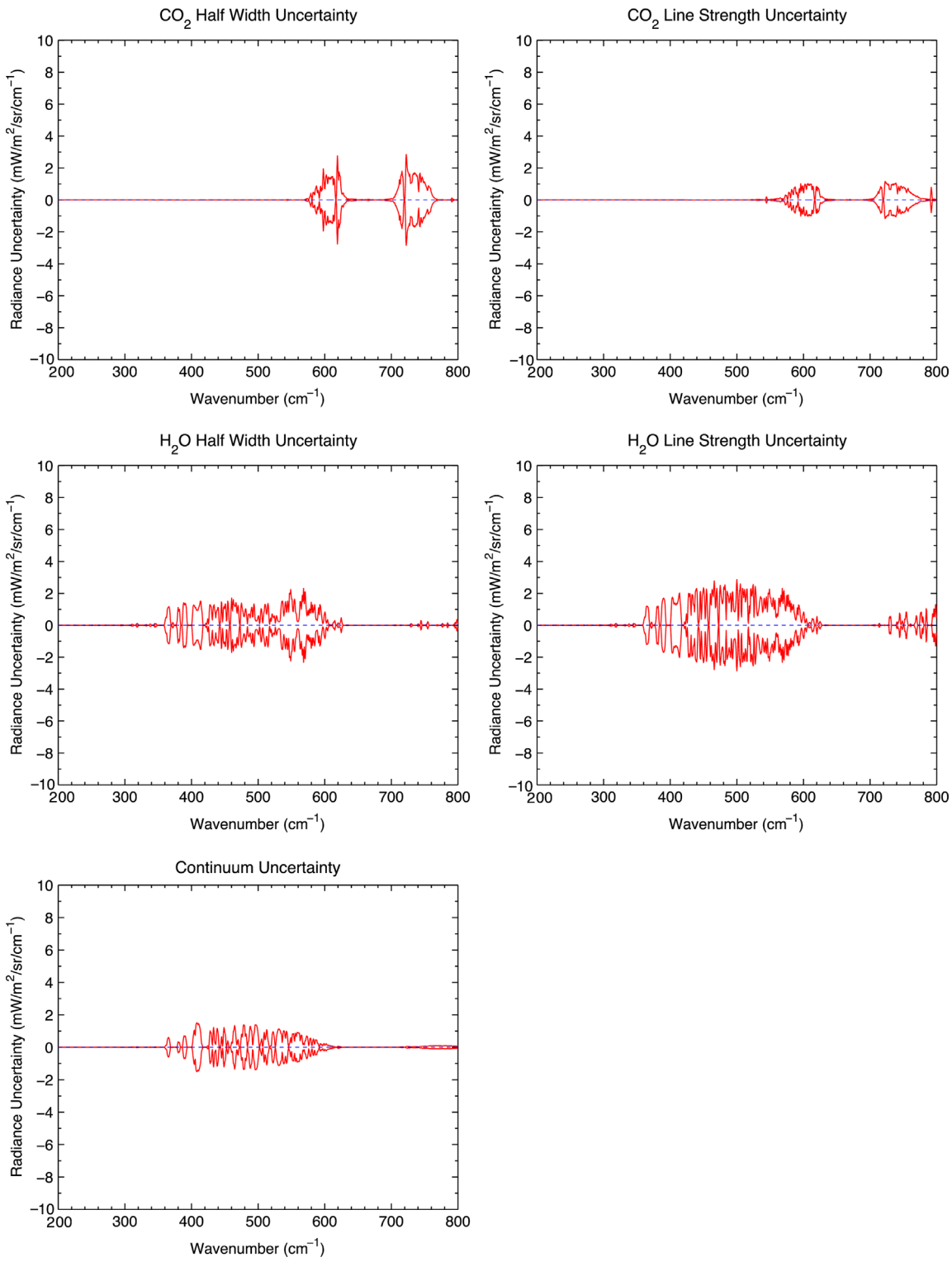

Fig. 12. Uncertainty in modeled radiances due to spectral line parameters of carbon dioxide (top) and water vapor (bottom), including uncertainty due to the water vapor continuum.

exceptional agreement within the optically thick regions from 200 to 360 cm^{-1} in the far-IR where water vapor dominates and between 620 and 720 cm^{-1} where carbon dioxide dominates.

The results shown in Fig. 16 demonstrate radiative closure between 200 and 800 cm^{-1}, over a range of brightness temperatures ranging from 189 K to 287 K (Fig. 6b). The differences between the modeled downwelling radiance

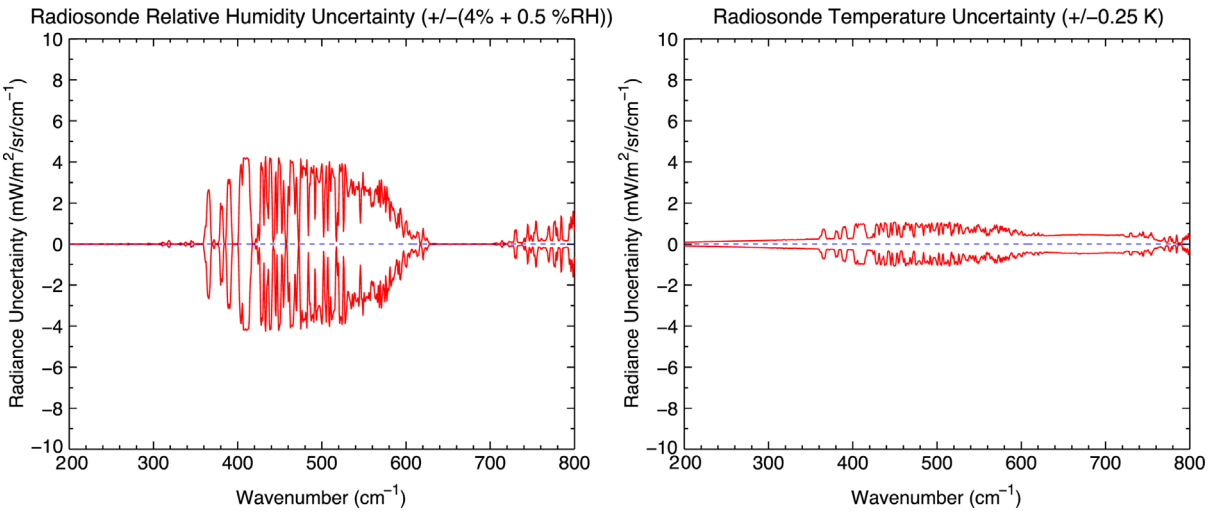

Fig. 13. Uncertainty in modeled radiance due to uncertainty in the radiosonde water vapor (left) and in the radiosonde temperature.

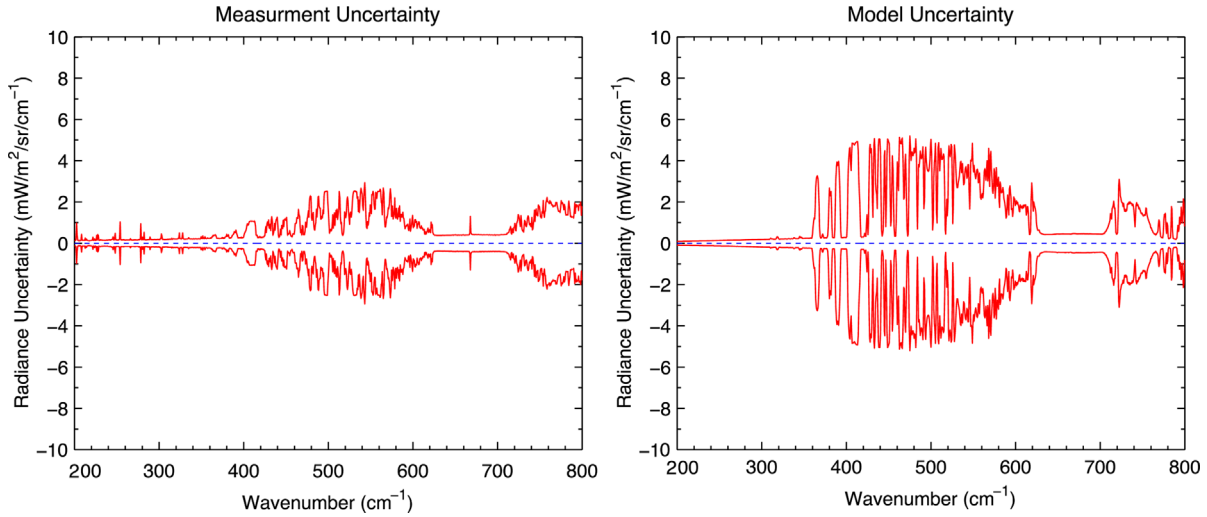

Fig. 14. Total measurement uncertainty (left) and total model uncertainty (right).

and FIRST measurements agree to within their combined uncertainty. From this aspect, we can conclude that radiative closure is achieved for this case study of FIRST data at Table Mountain on October 19, 2012. However the results would be much stronger if both the model and measurement uncertainties, and particularly the water vapor uncertainty, were smaller.

8. Summary and discussion

We have reported results of a radiative closure campaign conducted at the Table Mountain Facility, California, in autumn 2012. Observations of the downwelling infrared radiance from 200 to 800 cm^{-1} (50–12.5 μm) were made with the FIRST instrument. Substantial spectral development was observed between 360 and 620 cm^{-1} in the far-infrared. Simultaneous observations of temperature and water vapor made with radiosondes provide input to a radiative transfer model to produce modeled radiances for comparison with the observations. A detailed consideration of measurement and model uncertainty has been presented in order to properly assess the difference between the measured and modeled radiances. FIRST observations and model calculations have been shown to agree to within their combined uncertainty over the several hours of an observation campaign on 10/19/2012, at which time the integrated precipitable water was under 0.3 cm (3 mm). As such, we can conclude that the measurement and models demonstrate radiative closure on this day at Table Mountain, although improved knowledge of the water vapor profile would allowed stronger scientific conclusions to be drawn from the measurement campaign.

The FIRST instrument was developed to demonstrate technology to measure the far-IR spectrum in future space

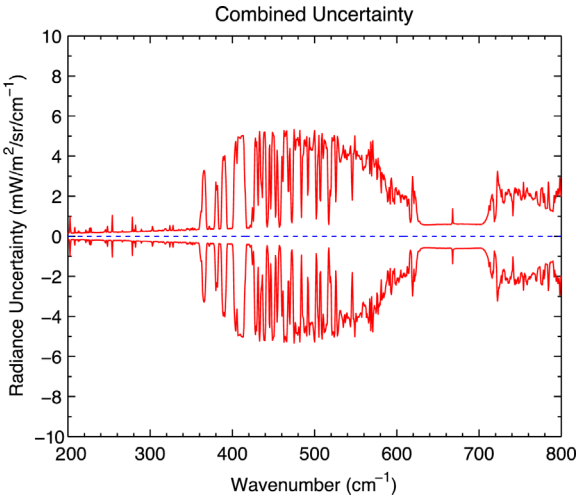

Fig. 15. Combined uncertainty of LBLRTM modeled radiances and FIRST measurements. This is the uncertainty to be compared against the residual of the LBLRTM modeled radiance and the FIRST measured radiance.

flight instruments. As such, achieving exceptionally high accuracy was not a goal of the instrument development effort, as is evident from the measured accuracy of the instrument shown in Table 1. Nevertheless, Figs. 12 and 14 show that the uncertainty in calculated radiance due to uncertainty in the line strengths and half-widths of water vapor and carbon dioxide are comparable to the FIRST calibration accuracy. Thus, even without a large uncertainty in water vapor, the results presented here demonstrate that the far-IR can be measured more accurately than it can be modeled. This is a critical point since one reason far-IR measurements have not been made from space since 1970 is due to a perception that it is sufficient to compute the far-IR spectrum from temperature and water vapor profiles retrieved from mid-IR measurements from space based sensors. Our results suggest the opposite is true, and that calculations alone are not sufficient to provide detailed scientific understanding of the far-IR and its role in climate. This is especially true in light of proposed future sensors such as the CLARREO infrared

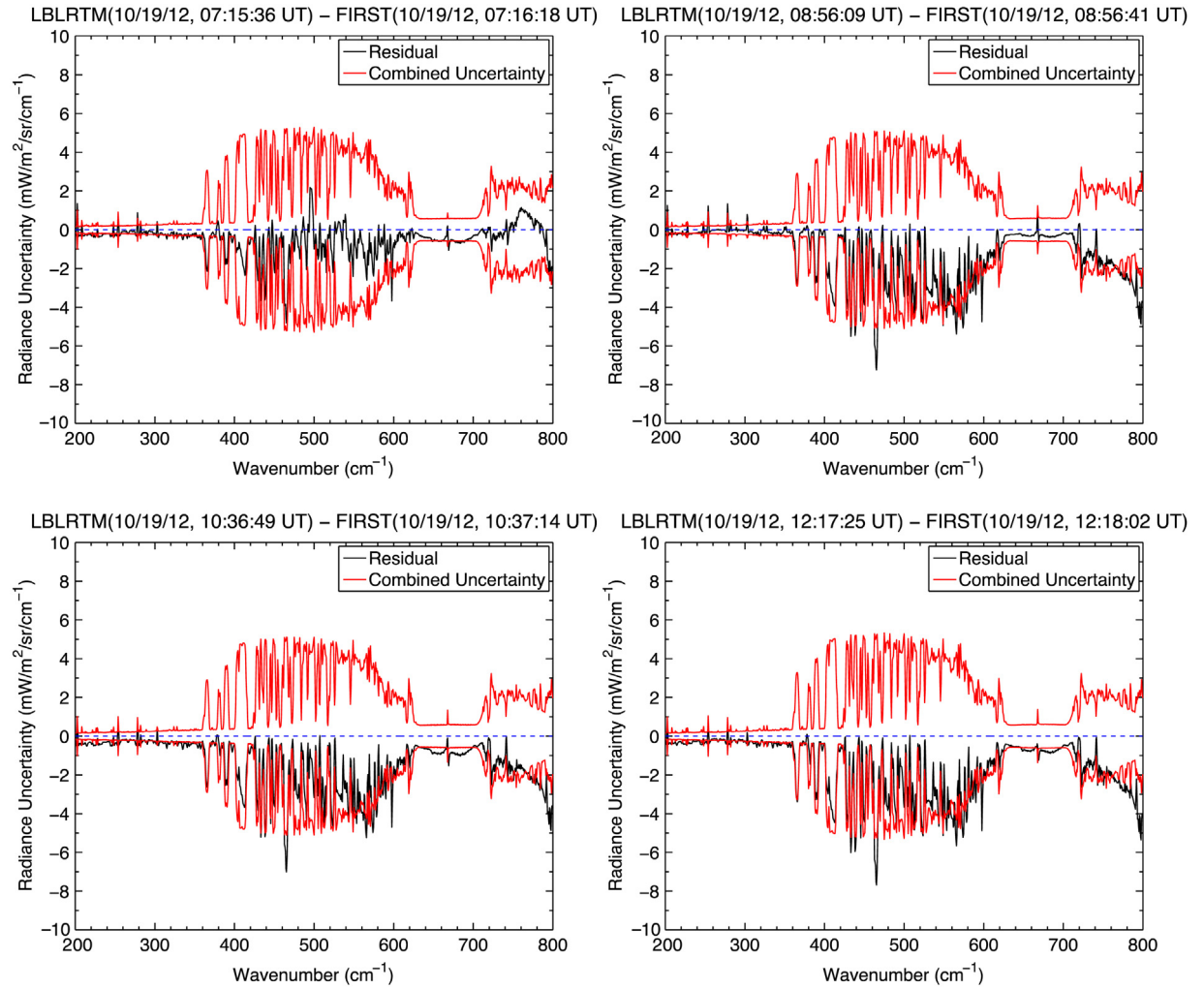

Fig. 16. FIRST measurement residuals and combined measurement uncertainty corresponding to the residuals shown above in Fig. 11.

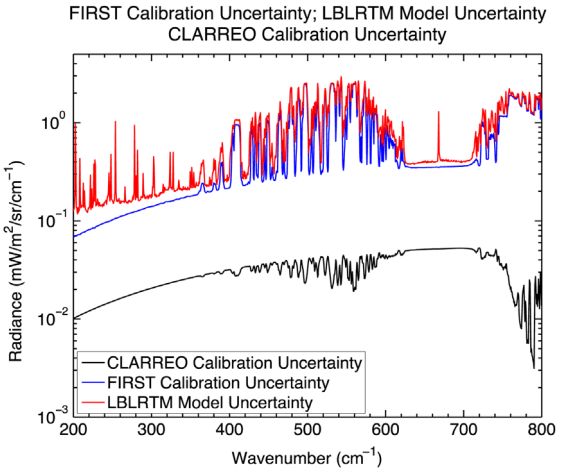

Fig. 17. Uncertainty in modeled radiance and FIRST measurements (from Fig. 14) along with the anticipated measurement uncertainty of the proposed CLARREO infrared sensor.

spectrometer [14] that, between 5 and 50 μm, will have an accuracy of 0.033 K (1-sigma, and 10 to 30 times better than FIRST) over all scene temperatures.

Fig. 17 shows the uncertainty in the modeled radiance at Table Mountain, the uncertainty of the FIRST measurements, and the anticipated CLARREO uncertainty, all expressed in units of radiance.

The expected CLARREO uncertainty, which is based on the accuracy necessary to detect climate trends [14], is well over an order of magnitude smaller than either the FIRST or modeled uncertainty. Many of the individual uncertainties in modeling radiance in the far-IR presented above correspond to several percent in radiance. Even with improvements in spectroscopy, it is anticipated that modeled radiance uncertainty in the far-IR may never approach or rival the measurement uncertainty that can now be achieved from space-based sensors. We are at present conducting an uncertainty analysis of top-of-atmosphere measurements of the far-IR spectrum for the purpose of assessing this conjecture. It does seem clear, however, that direct space-based measurements of the far-IR, rather than calculations alone, are essential to understand the climate system in detail.

Acknowledgements

The authors acknowledge the NASA Earth Science Technology Office for support of the FIRST recalibration effort and the Climate Absolute Radiance and Refractivity Observatory (CLARREO) project at NASA Langley Research Center for support of the FIRST field campaign data analyses. Dan Walsh, Thierry Leblanc, Pam Glatfelter, and Bruce Williamson of the Jet Propulsion Laboratory Table Mountain Facility were extremely helpful in making the deployment during August to October 2012 run smoothly. Jason Swasey, Kendall Johnson, Mark Esplin, Erik Syrstad, Mike Watson of the Space Dynamics Laboratory provided significant on-site support in the set up and operation of the FIRST instrument during the campaign.

References

[1] Aumann HH, Chahine MT, Gautier C, Goldberg MD, Kalnay E, McMillin LM, Revercomb H, Rosenkranz PW, Smith WL, Staelin DH, Strow LL, Susskind J. AIRS/AMSU/HSB on the aqua mission: design, science objectives, data products, and processing systems. IEEE Trans. Geosci. Remote Sens. 2003;41(2): 253–64. http://dx.doi.org/10.1109/TGRS.2002.808356.

[2] Hilton F, Coauthors. Hyperspectral earth observations from IASI: five years of accomplishments. Bull. Am. Meteor. Soc. 2012;93:347–70.

[3] Han Y, et al. Suomi NPP CrIS measurements, sensor data record algorithm, calibration and validation activities, and record data quality. J. Geophys. Res. Atmos. 2013;118(12): 734–48. http://dx.doi.org/10.1002/2013JD020344.

[4] Palchetti. L, Bianchini G, Castagnoli F, Carli B, Serio C, Esposito F, Cuomo V, Rizzi R, Maestri T. Breadboard of the Fourier-transform spectrometer for the Radiation Explorer in the Far Infrared (REFIR) atmospheric mission. Appl. Opt. 2005;44(14):2870–8.

[5] Canas A, Murray JE, Harries JE. The Tropospheric Airborne Fourier Transform Spectrometer (TAFTS). In: Proceedings of the SPIE3220, satellite remote sensing of clouds and the atmosphere II; 1997. p. 91–102.

[6] Mlynczak MG, et al. First light from the Far-Infrared Spectroscopy of the Troposphere (FIRST) instrument. Geophys. Res. Lett. 2006;33: L07704.

[7] Knuteson RO, Revercomb HE, Best FA, Ciganovich NC, Dedecker RG, Dirkx TP, Ellington SC, Feltz WF, Garcia RK, Howell HB, Smith WL, Short JF, Tobin DC. Atmospheric emitted radiance interferometer. Part I: instrument design. J. Atmos. Ocean. Technol. 2004;21:1763–76.

[8] Harries J, Carli B, Rizzi R, Serio C, Mlynczak M, Palchetti L, Maestri T, Brindley G, Masiello G. The far-infrared Earth. Rev. Geophys. 2008;46:RG4004. http://dx.doi.org/10.1029/2007RG000233.

[9] Mlynczak Martin G, Harries John E, Rizzi Rolando, Stackhouse Paul W, Kratz David P, Johnson David G, Mertens Christopher J, Garcia Rolando R, Soden Brian J. Far-infrared: a frontier in remote sensing of Earth's climate and energy balance. Proc. SPIE 2002;4485: 150. http://dx.doi.org/10.1117/12.454247.

[10] Kratz DP. High resolution modeling of the far-infrared. In: Proc. SPIE 4485, optical spectroscopic techniques, remote sensing, and instrumentation for atmospheric and space research IV, 30 January 2002; doi: 10.1117/12.454249.

[11] Clough SA, Iacono MJ, Moncet J-L. Line-by-line calculations of atmospheric fluxes and cooling rates: application to water vapor. J. Geophys. Res. 1992;97(D14):15761–85. http://dx.doi.org/10.1029/92JD01419.

[12] Liou K-N. Influence of cirrus clouds on weather and climate processes: a global perspective. Mon. Weather Rev. 1986;114:1167–98.

[13] Huang Y, Leroy S, Gero PJ, Dykema J, Anderson J. Separation of longwave climate feedbacks from spectral observations. J. Geophys. Res. 2010;115:D07104. http://dx.doi.org/10.1029/2009JD012766.

[14] Wielicki B, et al. Achieving climate change absolute accuracy on orbit. Bull. Am. Meteorol. Soc. 2013;94:1519–39. http://dx.doi.org/10.1175/BAMS-D-12-00149.1.

[15] Latvakoski H, Mlynczak MG, Johnson DG, Cageao RP, Kratz DP. Far-Infrared Spectroscopy of the Troposphere (FIRST) – calibration with a cold background. Appl. Opt. 2014;53:5425–33.

[16] Latvakoski H, Mlynczak MG, Johnson DG, Cageao RP, Kratz DP, Johnson K. Far-Infrared Spectroscopy of the Troposphere (FIRST) – instrument description and calibration performance. Appl. Opt. 2013;52:264–73.

[17] Turner DD, Mlawer EJ, Bianchini G, Cadeddu MP, Crewell S, Delamere JS, Knuteson RO, Maschwitz G, Mlynczak M, Paine S, Palchetti L, Tobin DC. Ground-based high spectral resolution observations of the terrestrial thermal spectrum under extremely dry conditions. Geophys. Res. Lett. 2012;39:L10801. http://dx.doi.org/10.1029/2012GL051542.

[18] Datla R., et al. NIST thermal-infrared transfer radiometer (TXR) deployments to measure the emissivity and radiance of the LWIRCS and GOES-R ECT blackbodies. In: Presented at 2011 CALCON technical conference in Logan, Utah; 29 August–1 September, 2011.

[19] Clough SA, Shephard MW, Mlawer EJ, Delamere JS, Iacono MJ, Cady-Pereira K, Boukabara S, Brown PD. Atmospheric radiative transfer modeling: a summary of the AER codes, short communication. J. Quant. Spectrosc. Radiat. Transf. 2005;91:233–44.

[20] Kratz DP, Mlynczak MG, Mertens CJ, Brindley H, Gordley LL, Martin-Torres J, Miskolczi FM, Turner DD. An inter-comparison of far-infrared line-by-line radiative transfer models. J. Quant. Spectrosc. Radiat. Transf. 2005;90:323–41.

[21] Kratz DP, Gao B-C, Kiehl JT. A study of the radiative effects of the 9.4 and 10.4 μm bands of carbon dioxide. J. Geophys. Res. 1991;96 (D5):9021–6.

[22] Miloshevich L, Vomel H, Whiteman D, Leblanc T. Accuracy assessment and correction of Vaisala RS92 radiosonde water vapor measurements. J. Geophys. Res. 2009. http://dx.doi.org/10.1029/2008JD011565.

[23] Coudert LH, Wagner G, Birk M, Baranov Yul, Lafferty WJ, Flaud J-M. The $H_2^{16}O$ molecule: line position and line intensity analyses up to the second triad. J. Mol. Spec. 2008;251: 339–57. http://dx.doi.org/10.1016/j.jms.2008.03.021.

[24] Kratz DP. The sensitivity of radiative transfer calculations to the changes in the HITRAN database from 1982 to 2004. J. Quant. Spectrosc. Radiat. Transf. 2008;109:1060–80. http://dx.doi.org/10.1016/j.jqsrt.2007.10.010.

[25] Delamere JS, Clough SA, Payne VH, Mlawer EJ, Turner DD, Gamache RR. A far-infrared radiative closure study in the Arctic: application to water vapor. J. Geophys. Res. 2010;115: D17106. http://dx.doi.org/10.1029/2009JD012968.

[26] Fox C, Green P, Pickering JC, Humpage N. Analysis of far-infrared spectral radiance observations of the water vapor continuum in the Arctic. J. Quant. Spectrosc. Radiat. Trans. 2015;155: 57–65. http://dx.doi.org/10.1016/j.jqsrt.2015.01.001.